PREPRINT UCRL-77743

CONF-760828--8

Lawrence Livermore Laboratory

TIME RESOLVED X-RAY PINHOLE PHOTOGRAPHY OF COMPRESSED LASER FUSION TARGETS

D. T. Attwood

July 26, 1976

This paper was prepared for presentation at
12th International Congress on High Speed Photography
August 1-7, 1976, Toronto, Canada

TIME RESOLVED X-RAY PINHOLE PHOTOGRAPHY OF COMPRESSED LASER FUSION TARGETS*

D. T. Attwood
Lawrence Livermore Laboratory, University of California
Livermore, California 94550

Abstract

In this paper we discuss use of the Livermore x-ray streak camera to temporally record x-ray pinhole images of laser compressed targets. Use is made of specially fabricated composite x-ray pinholes which are near diffraction limited for 6 Å x-rays, but easily aligned with a He-Ne laser of 6328 Å wavelength. With a 6 μm x-ray pinhole, the overall system can be aligned to 5 μm accuracy and provides implosion characteristics with space-time resolutions of approximately 6 μm and 15 psec. Acceptable criteria for pinhole alignment, requisite x-ray flux, and filter characteristics are discussed. Implosion characteristics are presented from our present experiments with 68 μm diameter glass microshell targets and 0.45 terawatt, 70 psec Nd laser pulses. Final implosion velocities in excess of 3×10^7 cm/sec are evident.

Introduction

Experiments designed to study laser driven implosions of glass microshells are underway in several laboratories around the world. The ultimate goal of these experiments is to drive the encapsulated deuterium-tritium fuel to a sufficiently high density and temperature that the resultant thermonuclear reaction produces a net energy gain [1, 2]. In preliminary experiments it has been shown that modest compressions are achieved [3], and that the resulting neutrons are of a thermonuclear origin [4]. It is important that these early experiments be understood in sufficient detail that future experiments can be accurately designed. Because of the high densities and temperatures involved, x-ray emission from the compressed target provides a primary source of data regarding dynamics of the implosion process. A typical implosion experiment involves an approximately 100 micron initial diameter target which implodes to a fraction of its initial size on a time scale of roughly 100 picoseconds. The x-ray data must therefore be resolved spatially to microns and temporally to several picoseconds in order to provide direct data describing the heating and implosion processes. However, diagnostics available to date have not had the capability of simultaneously providing the required space-time resolutions. Time integrated x-ray imaging studies provide spatially resolved photographs showing target compression [3, 5]. Spatially integrated streak camera studies provide temporally resolved x-ray spectral signals interpretable in terms of implosion times [6, 7]. In this paper we report the first temporally resolved x-ray images of laser compressed targets with sufficient resolution to continuously follow the implosion process. The resultant space-time characteristics provide directly observable implosion velocities, and as such provide direct, detailed data of the type required for meaningful comparison with numerical simulations.

Image Formation and Detection

In a companion paper [6] we discussed use of our 15 picosecond x-ray streak camera to record spectrally and temporally resolved x-ray emission from laser compressed targets. Here we discuss the extension of that work to time resolved pinhole photography [8]. A schematic diagram of the general concept appears in Figure 1. An x-ray pinhole is used to image the target, with its own x-ray emission, on the slit of the streak camera. The one dimensional image seen by the slit-shaped cathode is then streaked in time, giving a space-time history of the target implosion. The imaging system must be chosen such that a spatially well resolved, accurately aligned x-ray image illuminates the photocathode. In addition, the image must be of detectable intensity.

As indicated above, x-ray pinholes are used in the work reported here, primarily because they combine ease of construction and large magnification with reasonable spatial resolution. It is well known that x-ray pinhole cameras can provide spatial resolutions in the micron range when properly designed with respect to geometrical and diffractive effects. For given wavelength λ and object distance p, the optimum pinhole diameter d, for a large magnification camera, is given by [9-15]

$$d \simeq 1.6 \sqrt{\lambda p} \qquad (1)$$

For 2 keV x-rays ($\lambda \simeq 6$ Å) and an object distance p of 1 cm, the optimum pinhole diameter is approximately 4 μm. For smaller pinhole diameters obtainable spatial resolution

* Work performed under the auspices of the the United States Energy Research and Development Administration under contract No. W-7405-Eng-48.

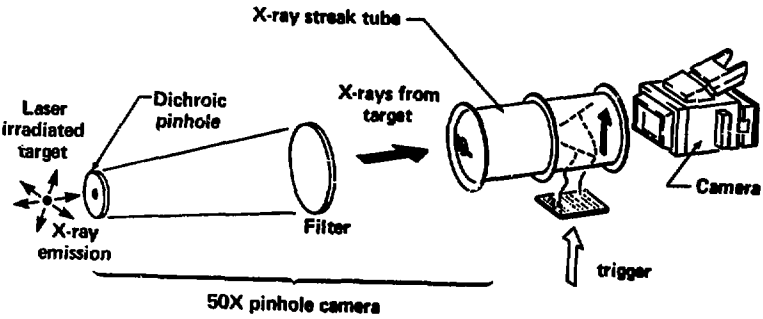

Figure 1. Schematic diagram showing the laser irradiated target, a 50x pinhole camera, and a simplified representation of the x-ray streak camera. Note that a vertical target displacement of one radius from the ideal position renders the image tangential to the slit shaped cathode, and therefore undetectable.

is seriously degraded by diffraction. For larger pinholes, spatial resolution is essentially given by the pinhole diameter. In the work presented here, a 6 μm diameter x-ray pinhole is employed.

It is evident upon inspection of Figure 1 that a vertical displacement of one target radius from the optimum position renders the image tangential to the streak camera slit and therefore unphotographable. Considering that we are interested in 60 - 100 μm diameter targets, and that these implode to a fraction of their initial radius, severe requirements on alignment accuracy are imposed, typically of several microns. The difficulty that this generates resides in the fact that the x-ray pinholes are chosen to be near diffraction limited at 6 Å, and a sufficiently intense alignment source does not exist at that wavelength. Instead we seek to use a convenient visible alignment technique employing a CW He-Ne laser at 6328 Å. For the given geometry and near optimum x-ray pinhole diameter, this factor of 1000 difference in wavelength causes severe diffraction and essentially renders the visible alignment source useless. A solution to this apparent conflict is to construct composite pinholes [16] which appear small to x-ray wavelengths, but large to visible wavelengths. The use of x-ray absorbing, visibly transparent glass to construct such pinholes is discussed in the following section. An alignment scheme, accurate to approximately 5 μm, is also presented.

In addition to image formation and alignment, there is also the significant question of x-ray intensity within the image vis-à-vis detection limits. A conservative estimate of detectability can be made on the basis of previous streak records without imaging and use of a simple model of spatially uniform but time dependent x-ray emission [17]. With such an emission model one easily shows, that for a large magnification pinhole camera, the x-ray intensity at the streak camera slit is reduced, with respect to the unimaged case, by an intensity loss factor,

$$\beta = \left(\frac{d}{D}\right)^2 \qquad (2)$$

where d is the pinhole diameter and D is the target diameter. We now use this model to estimate x-ray flux levels at two times: an early heating phase before significant target compression, and a later peak compression period when the target diameter is at its smallest value. According to reference 6 (Fig. 8 and accompanying text) the low energy channel for a half terawatt experiment shows pre-compression flux levels a factor of 100 above detection limits, while peak compression levels are nearly a factor of 1000 above such limits. Considering a pinhole diameter d=6 μm, an initial target diameter D_i of 60 μm, one expects pre-compression flux levels to be reduced with imaging (see Eq. 2) by a factor of 100, rendering them just barely detectable in these experiments. At later times, near peak compression, the final target diameter D_f is expected to be approximately 8 μm, giving a loss factor β of only two. Since flux levels are relatively high and losses are minimal, we conclude that the period of peak compression is easily recorded with our x-ray

streak camera, a 6 μm pinhole, and a half terawatt of laser energy on a 60 μm diameter glass shell target.

Pinhole Design and Alignment

As mentioned in the previous section, the crucial feature of these experiments is pinhole-target alignment. With 60 μm diameter targets compressed to a fraction of their initial size, alignment accuracies of several microns are required to keep the x-ray image centered on the slit cathode of the streak camera. With pinhole sizes chosen to be near diffraction limited for 6 Å x-rays, it is evident that composite pinholes [15, 16] are required to permit simple alignment, with a 6328 Å He-Ne laser. Such pinholes appear appropriately small at x-ray wavelengths, but considerably larger and not overly diffracting for the visible alignment source. A typical composite pinhole is shown in Figure 2.

Figure 2. A typical composite pinhole is mounted on the end of a 16 gauge hypodermic needle, as shown in (a). A 125 micron diameter hole is mechanically drilled in a 12 micron thick gold foil, and then covered with a thin (5-10 micron thick) layer of x-ray absorbing, visibly transparent glass. A smaller (3-10 micron) x-ray pinhole is then laser drilled concentrically with the larger hole as shown in (b). A scanning electron microscope picture of the laser drilled hole is shown in (c). Composite pinholes have been formed with both tungsten phosphate and tantalum silicate glasses.

It is fabricated by first mounting a 12 μm thick gold foil on the end of a 16 gauge hypodermic needle, as seen in Figure 2 (a). A 125 μm diameter hole is mechanically drilled in the gold foil and then the entire gold foil is covered in this case with a 9 μm thick disc of 66% by weight tungsten phosphate glass [18]. This glass has an x-ray absorptance of 10^{-1} in the spectral region of interest, and a visible transmittance of 13%. A 7 μm diameter hole is then laser drilled concentrically with the larger 125 μm diameter hole, as shown in Figure 2 (b). A closeup view of the x-ray pinhole, taken with a scanning electron microscope, is shown in Figure 2 (c). Pinholes in the 3-10 μm diameter range have been constructed in the tungsten phosphate glass and also in 20 μm thick tantalum silicate glass [19]. The latter exhibits higher x-ray absorptance and higher visible transmittance than the tungsten glass, but has a higher melting point and is therefore more difficult to work with. High concentration lead glasses have not been used because lead has an M-edge at 2.48 keV and thus allows x-ray leakage, or insufficient absorptance in that spectral region. Tungsten and tantalum have their respective M-edges at 1.81 and 1.74 keV.

The visible alignment scheme used in conjunction with composite pinholes is shown in Figure 3. A He-Ne laser, spatial filter, focusing lens and pellicle combine to provide the visible alignment beam. They are oriented in a way that the light appears to originate symmetrically from the center of the streak camera cathode. The pellicle is 50% reflective, 50% transmissive at 6328 Å, and 99% transmitting for x-rays of interest. The focal length of the lens is chosen to produce a focal region waist midway between pinhole and target. By appropriate clipping of the beam at the focusing lens, a set of Airy rings [20] modulate the waist pattern. The second dark ring is set approximately at 125 μm to allow accurate alignment of the large (125 μm) hole of the composite pinhole. The x-ray pinhole is now centered in the optical alignment pattern, within a concentricity error of 2 or 3 microns for the composite pinholes. The transmitted interference pattern, now somewhat affected by pinhole diffraction, propogates on to the target plane one centimeter away. The target is then moved to a central position as shown in the successive photographs of Figure 4. With the cathode slit, pinhole, and target in alignment, the system is ready for target irradiation and compression experiments.

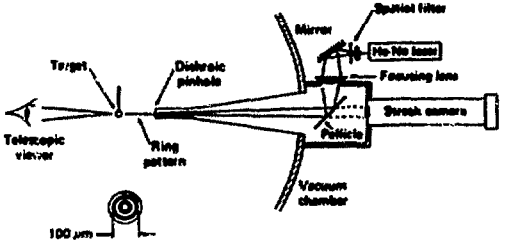

Figure 3. Target alignment scheme employing a He-Ne laser, a focusing lens, and a set of Airy rings. Both the composite pinhole and the target are centered in the visible diffraction pattern.

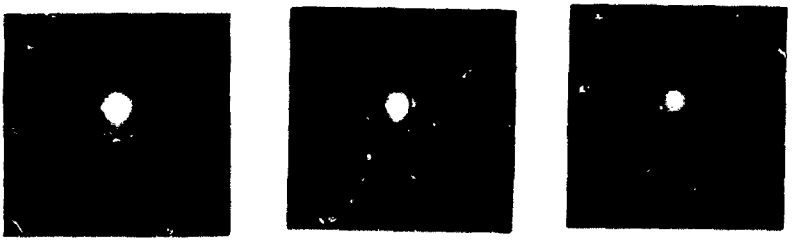

Figure 4. Three steps to easy target alignment via use of the Airy diffraction pattern described in Figure 3. The successive photographs show the target being moved to a central position where it will be properly aligned with both the pinhole and x-ray streak camera cathode.

Space-Time Implosion Diagrams

Results obtained during recent implosion experiments with Livermore's JANUS laser facility [1-3] are presented in Figures 5 - 7 for three nearly identical targets. These experiments involved the irradiation and compression of typically 68 micron diameter 0.5 micron thick DT filled glass microshells. Using ellipsoidal focusing mirrors (NA=0.99), the laser delivered approximately 0.45 TW in a typical 70 psec, two-sided irradiation experiment. X-ray imaging and filtering were obtained with a 6 micron diameter tantalum pinhole and a 125 micron thick beryllium filter, respectively. The space-time implosion diagrams presented in Figures 5-7 show isodensity film contours obtained directly from the respective

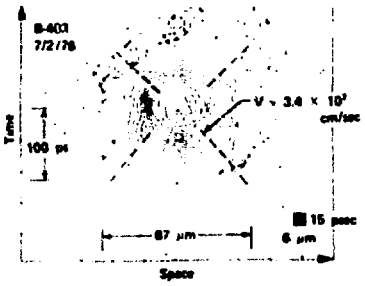

Figure 4. Isodensity contours obtained from x-ray pinhole/streak record. The target had a wall thickness of 0.51 microns, a DT fill of 1.32 mg/cc, and upon irradiation produced 1 x 10^6 neutrons. Two sided target irradiation consisted of 17.2J and 16.6J, 75 psec FWHM pulses.

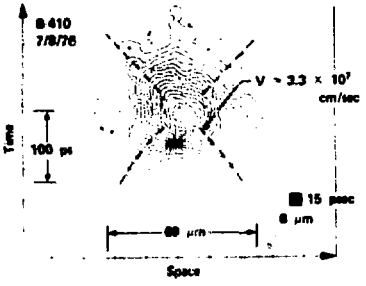

Figure 6. Isodensity contours obtained directly from x-ray pinhole/ streak record. The target had a wall thickness of 0.44 microns, a DT fill of 1.67 mg/cc, and upon irradiation produced 1 x 10^6 neutrons. Two sided target irradiation consisted of 14.6J and 16.6J, 64 psec FWHM pulses.

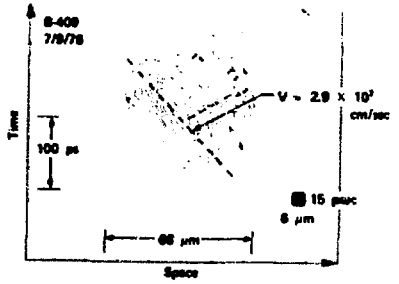

Figure 7. Isodensity contours obtained directly from x-ray pinhole/streak record. The target had a wall thickness of 0.57 microns, a DT fill of 1.82 mg/cc, and upon irradiation produced 2 x 10^5 neutrons. Single sided target irradiation consisted of a 16.9J pulse of approximately 70 psec FWHM.

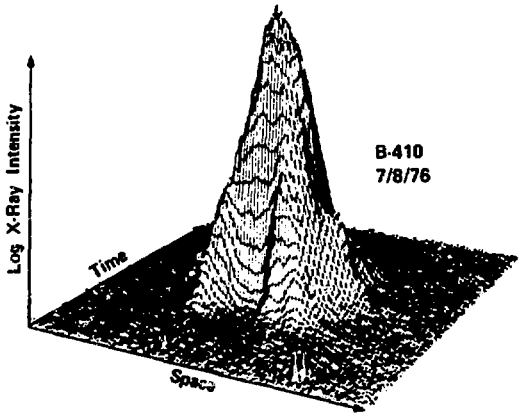

Figure 8. Isometric presentation of the space-time isodensity contours for the implosion of target B-410, Figure 6. Low intensity x-ray emission at the early time periphery, and intense emission at the later time compressed core, are easily identified.

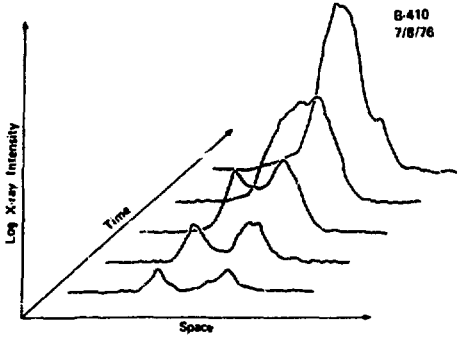

Figure 9. Spatial profiles showing the implosion of B-410 at various times. This data is obtained by examining various iso-temporal planes in Fig. 8. Emission from opposite sides of the imploding shell are observed to coalesce and finally form an intense stagnation region near the target center.

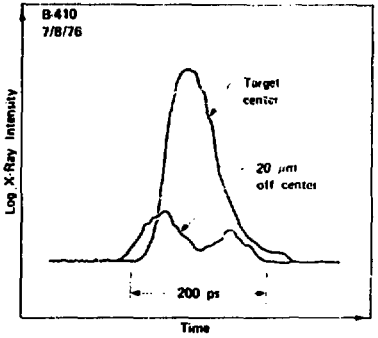

Figure 10. Temporal profiles of x-ray emission from the target center and from a position 20 microns to one side. The latter shows a double humped behavior as intense x-ray emission passes this radial position once during implosion and once during post-compression disassembly. This data is obtained by examining iso-spatial planes in Figure 8.

pinhole/streak camera records. Shaded blocks in the lower right hand corner of each diagram display the approximate space-time resolutions of 6 microns and 15 picoseconds.

The results presented in Figures 5 and 6 show two rather similar implosions, except that one is somewhat more symmetric (Figure 5), while the other shows more pronounced details of target acceleration. Both produced final implosion velocities [24] of approximately 3.4×10^7 cm/sec, as seen in the illustrations. Further details from these two-sided irradiation experiments are presented in the following paragraph. In the third experiment, described by Figure 7, target irradiation was purposely blocked on one side so as to observe details of a single sided implosion experiment. This one sided irradiation experiment is very interesting in that it shows a hydrodynamically focused implosion at the target center, and an asymmetric but two sided disassembly as the compressed core coasts for some distance beyond the target center.

Taking target B-410, Figure 6, as representative of these implosion experiments we describe it further in Figures 8 - 10. Figure 8 shows an isometric presentation of the film density, which is proportional to x-ray intensity, as a function of space and time coordinates. This type of presentation is employed as it is somewhat easier to visualize the simultaneous space-time compression in this form. Taking planar cuts of the data in Figure 8 at discrete times and spatial positions we obtain the profiles presented in Figures 9 and 10. Figure 9 shows spatial contours of x-ray emission at several discrete times. At an early time the spatial profile shows two distinct emission regions corresponding to the oppositely directed sides of the imploding shell. At a later time, but before peak compression, the two regions grow significantly in intensity and begin to coalesce. At a still later time the two regions have merged into a single, stagnated core of peak x-ray intensity. Final target disassembly in the post-compression period is omitted for clarity.

Figure 10 shows x-ray temporal profiles for the target center, and for a position 20 microns off center. Note that the latter position displays a two humped behavior as peak radiation passes that radial position once during implosion and once during disassembly. Note that a properly weighted sum of the two temporal profiles in Figure 8 could be used effectively to reconstruct the unimaged profiles presented in Reference 6. Further analysis of these results is underway, particularly with respect to removal of recording film (D vs. log E) characteristics. Experiments in other regions of parameter space are also in progress.

Summary

Requirements for time resolved x-ray pinhole photography have been reviewed with particular emphasis on spatial resolution, pinhole alignment accuracy, and required emission levels. Pertinent data regarding the Livermore 15 picosecond streak camera are reviewed. Special techniques employing composite, or dichroic, pinholes have been described which permit simple and accurate positioning of micron size x-ray pinholes. Results with space-time resolutions of approximately 6 microns and 15 picoseconds are presented which clearly show the implosion of laser irradiated 68 micron diameter glass microshell targets. Shell acceleration, culminating in a final implosion velocity of greater than 3×10^7 cm/sec, is evident for both single and double sided irradiation experiments.

Acknowledgments

The author acknowledges numerous conversations and the consistent support of L. W. Coleman throughout this project. Members of the Laser/Plasma Interactions group who conducted the implosion experiments are gratefully acknowledged, particularly D. W. Phillion, J. E. Swain, K. Manes and H. G. Ahlstrom. C. H. Dittmore provided valuable assistance in the reduction of data. R. F. Wuerker, B. W. Weinstein, G. E. Sommargren, J. W. Houghton, B. Holloway, S. Nakano, E. R. Prochnow, J. Shelby and D. Blackburn have each played significant roles in constructing the x-ray pinhole camera. J. T. Larsen provided many useful discussions of the implosion process. Targets for these experiments were provided under the direction of C. D. Hendricks.

References

1. J. Nuckolls, L. Wood, A. Thiessen and G. Zimmerman, Nature 239, 139 (1972).
2. J. L. Emmett, J. Nuckolls, L. Wood, Sci. Amer. 230, 24 (1974).
3. P. M. Campbell, G. Charatis, and G. R. Monty, Phys. Rev. Lett. 34, 74 (1975).
4. V. W. Slivinsky, H. G. Ahlstrom, K. O. Tirsell, J. T. Larsen, S. Glaros, G. Zimmerman and H. Shay, Phys. Rev. Lett. 35, 1083 (1975).
5. F. Seward, J. Dent, M. Boyle, L. Koppel, T. Harper, P. Stoering and A. Toor, Rev. Sci. Inst. 47, 464 (1976).
6. D. T. Attwood and L. W. Coleman, XII Intl. Conf. on High Speed Photography, paper DA-1, Toronto, 1976; Bull. Amer. Phys. Soc. 20, 1267 (1975).
7. D. T. Attwood, L. W. Coleman, J. T. Larsen and E. K. Storm, accepted Phys. Rev. Lett.
8. In several respects use of an x-ray microscope is preferable for these studies. For instance, large numerical aperture and high spatial resolution are achievable with large object distances. The latter is important both for convenience and resistance to damage from unabsorbed laser light, reaction products, and general target debris.

References (cont)

However, as reported in Reference 6, the x-ray streak camera has a spatial resolution of 130 um at the cathode, necessitating use of a 50x imaging system to obtain reasonable spatial resolution in the target plane. Large magnification x-ray microscopes are presently being constructed at Livermore under the direction of M. Boyle and H. Ahlstrom.

9. B. M. Kovinsky and V. G. Lutsau, appearing in X-Ray Microscopy and Microradiography, edited by V. Cosslett et. al. (Academic, New York, 1957), p. 131. These authors obtained 1 micron spatial resolution in well designed x-ray pinhole experiments
10. R. P. Godwin, appearing in Advances in X-Ray Analysis, edited by R. Gould (Kendall/Hunt, Dubuque, Iowa, 1975), p. 560.
11. G. Reynolds and J. Ward, J. Soc. Phot. Instr. Eng. 5, 3 (1966).
12. R. Swing and D. Mooney, J. Opt. Soc. Amer. 58, 629 (1968).
13. J. Mack and K. Martin, The Photographic Process (McGraw-Hill, New York, 1939), p. 47.
14. S. Tolansky, Curiosities of Light Rays and Light Waves (American Elsevier, New York, 1965), p. 12.
15. D. T. Attwood, B. W. Weinstein and R. F. Wuerker, in preparation.
16. D. T. Attwood, USAEC Patent Disclosure UI-5954 (May 17, 1976).
17. This of course is not an accurate model since spatial and temporal non-uniformities clearly exist, as discussed in this paper. However, consideration of this model at two distinct times, early heating and peak compression, allows us to make simple prediction of required flux levels. In the sense that departures from uniformity are more easily detected, these estimates will be conservative in nature.
18. J. J. Rottermel, K. H. Sun, and A. Silverman, J. Am. Ceram. Soc. 57, 1 3 (1974).
19. The composition of this glass is 60% TaO_5, 20% Ba O, 13% Si O_2, and 7% H_2O by weight.
20. M. Born and E. Wolf, Principles of Optics (Pergamon, New York, 1975), p. 191.
21. J. F. Holzrichter and D. R. Speck, J. Appl. Phys. 47, 2450 (1976).
22. H. G. Ahlstrom and J. F. Holzrichter, Laser Focus 11, 33 (1975).
23. J. F. Holzrichter, H. G. Ahlstrom, D. R. Speck, E. Storm, J. E. Swain, C. W. Cranfield, C. D. Hendricks, H. H. Kornblum, F. D. Seward, V. W. Slivinsky, Y. C. Tan, J. P. Zimmerman, and J. H. Nuckolls, to be published in Plasma Physics.
24. These final velocities are consistent with indirect estimates of average piston velocity discussed elsewhere (References 6 and 7) when proper account is taken of target mass and absorbed laser energy.